

Modular memristor model with synaptic-like plasticity and volatile memory

Daniel Habart,^{1,*} Stephen H. Foulger,^{2,3,4} Kristyna Kovacova,¹ Ambika Pandey,⁵
Yadu R. Panthi,⁵ Jiří Pflieger,⁵ Jarmila Vilčáková,⁶ and Lubomir Kostal^{1,†}

¹*Institute of Physiology of the Czech Academy of Sciences,
Videnska 1083, 14200 Prague 4, Czech Republic*

²*Center for Optical Materials Science and Engineering Technologies (COMSET),
Clemson University, Clemson, SC 29634 USA*

³*Department of Materials Science and Engineering,
Clemson University, Clemson, SC 29634 USA*

⁴*Department of Bioengineering, Clemson University, Clemson, SC 29634 USA*

⁵*Institute of Macromolecular Chemistry, Czech Academy of Sciences,
Heyrovskeho nam. 2, 16206, Prague 6, Czech Republic*

⁶*Department of Physics and Materials Engineering,
Faculty of Technology, Tomas Bata University in Zlin,
Tr. T. Bati 5678, 760 01 Zlin, Czech Republic*

Abstract

Compact models of memristors are essential for simulating large-scale neuromorphic systems, yet they often do not include description of complex dynamics like volatile relaxation and synaptic plasticity. We introduce a modular, computationally efficient memristor model that bridges this gap by integrating principles from physics and computational neuroscience. The model defines a framework consisting of a standard formulation of memristive device dynamics, a functional rule mapping state variables to cumulative conductance, a volatility module inspired by the theory of linear viscoelasticity and a saturation module implementing a linear-nonlinear technique. Additionally, we develop a formulation of synaptic-like plasticity inspired by a biological spike-timing-dependent plasticity (STDP) rule, which is compatible with the general framework for memristive devices. Finally, we propose a Laplace transform-based technique to derive the precise form of the mapping from state variables to cumulative conductance, replacing ad hoc voltage-current relationships with principled construction.

We quantitatively validate the complete model against a rich set of experimental data from polymeric memristors exhibiting potentiation, synaptic-like plasticity and volatile decay. Our work presents a new paradigm for memristor modeling that is both practical for large-scale simulation and rich in explanatory power, providing a principled tool for the design of next-generation neuromorphic hardware.

I. INTRODUCTION

Neuromorphic computing allows physical devices to bring memory and computation closer together, targeting improvements in energy efficiency compared to traditional von Neumann architectures [1, 2]. Memristors, two-terminal devices whose conductance depends on the history of electrical stimulation [3, 4], are particularly well suited to serve as artificial synapses [5]. Their inherent memory, analog tunability, and scalability make them attractive for both fundamental studies and applications in neuromorphic hardware [1].

Compact models such as TEAM and VTEAM [6, 7] provide versatile descriptions of memristive switching [8], widely used in circuit-level simulations. However, for applications

* Contact author: daniel.habart@gmail.com; These authors contributed equally to this work.

† Contact author: lubomir.kostal@fgu.cas.cz; These authors contributed equally to this work.

in neural networks, additional properties such as volatility and synaptic-like plasticity must be accounted for in a quantitative and flexible manner. The recently proposed V-VTEAM model [9] addresses volatility of conductance by modifying the dynamics of the memristive system, differing from our approach. Volatile conductance relaxation, in particular, enables short-term memory and fading dynamics [10–12], while spike-timing-dependent plasticity (STDP) underlies learning and long-term adaptation [5, 13, 14].

Biological synapses inspire these features: transient responses decay unless reinforced, whereas repeated pre- and post-synaptic activity leads to long-term modifications. Importantly, STDP can be described in terms of local variables (eligibility traces) that evolve directly from the input spikes, making the mechanism both biophysically plausible and technically practical [15].

To capture memristor volatility, we take inspiration from linear viscoelasticity theory, where material stress depends on the convolution of strain differences with a hereditary kernel [16, 17]. In our case, the internal conductance state depends on the past applied voltage (or equivalently, passed charge) through a convolution with a kernel that decays approximately as $1/t$. This form reflects a broad distribution of relaxation times, consistent with disordered systems and percolation phenomena in which conduction pathways evolve stochastically over time [18, 19].

Our formulation is presented in a voltage-driven form, which is natural for many experimental setups. Nevertheless, thanks to the modular structure of the model, switching to a current-driven variant requires only minor adjustments and does not change the essential dynamics. This flexibility ensures broad applicability across device classes.

We propose a *modular memristor model* that unifies multiple modules :

1. a compact memristive component building on established voltage-based models [7, 20];
2. a novel STDP component based on local-variable eligibility traces [15], yielding biologically inspired causal and anti-causal weight updates;
3. a cumulative conductance function, establishing the relationship between evolution of state variables and conductance;
4. a volatility module inspired by viscoelastic hereditary convolution with a kernel;

5. a saturation module, which implements a linear-nonlinear scheme in conjunction with the volatility module to produce the resulting conductance.

A schematic representation of the model is provided in Figure 1. The model is quantitative, flexible, and computationally efficient. Its modularity allows enabling or disabling volatility and STDP without altering the core equations.

To demonstrate its applicability, we compare model dynamics with experimental data from polymeric memristors developed by Pflieger, Foulger, and co-workers [21–24]. This device consists of a thin film of poly(N-(3-(9H-carbazol-9-yl)propyl)methacrylamide) sandwiched between ITO and top metallic electrodes. The memristor showed pronounced hysteresis in its I-V characteristics. At higher voltages about ± 5 V it exhibits bistable resistive switching effects, with a maximum ON/OFF ratio of around 200 and good retention time exceeding 2 hours in both ON and OFF states [21]. At lower voltage range the device shows an analog behavior and its resistance, stimulated by a series of low amplitude voltage pulses, can gradually increase or decrease, similarly as the potentiation and depression of neuronal synapses [22].

We have additionally included a technique based on the Laplace transform to determine the functional form of the cumulative conductance function for the specific physical device under evaluation in IV C. Owing to the simplicity of the model framework, this form could provide insight to the characteristic macroscopic behavior of the device, dependent on the chosen memristor model.

We believe this approach will help bridge the gap between device-level physics and system-level neural computation, with particular relevance for sustainable, polymer-based memristive hardware.

II. MODEL

Our objective is to develop a modular model of a volatile memristor exhibiting spike-timing dependent plasticity (STDP) characteristics. We begin by presenting commonly used voltage-controlled memristor models. Next, we adapt an online synaptic STDP model into a form suitable for non-spiking one-port electronic devices. We draw inspiration from linear viscoelasticity [16] to model the observed volatility in device conductance, introducing a cumulative conductance function together with a decay kernel. Finally, we combine these

components and apply a linear-nonlinear technique [25] to both capture the conductance saturation observed in devices and to constrain the admissible conductance range.

A key advantage of our framework is its modularity. One may freely choose a memristor voltage-controlled model, the cumulative conductance function, the decay kernel and saturation function, subject to only minimal constraints, to best match the device being modeled.

For reference, we recall the general framework for voltage-controlled, time-invariant one-port memristive systems introduced by Chua and Kang [4]. Such a device is described by a differential equation governing the evolution of a vector of internal state variables \mathbf{x} , together with an algebraic equation relating the current and voltage through a conductance function $G(\mathbf{x})$:

$$\begin{aligned} i &= G(\mathbf{x})v \\ \dot{\mathbf{x}} &= f(\mathbf{x}, v). \end{aligned} \tag{1}$$

Here v is the voltage across the device, i is the current through the device and the functions f and G are such that we assume a unique solution to the equation. Throughout the following, the symbol $\dot{\cdot}$ always denotes differentiation with respect to time.

Our approach is inspired by the memristive system framework, but differs from it in several important aspects. Following Eq. (1), we introduce a vector of four internal state variables: s , w , x , y , along with a description of their respective dynamics. However, unlike in the formulation above, our conductance function G is not a direct function of the state parameters. Instead, we introduce an intermediate function H and compute the device conductance G using a linear–nonlinear approach combined with the linear viscoelasticity framework.

Namely, we introduce a kernel function $\ker(\cdot)$ to capture the temporal decay of conductance, a "cumulative conductance" function $H(s, w)$ to describe the non-volatile conductance characteristics and a saturation function $\text{sat}(\cdot)$ to model conductance saturation. A schematic of the modules' relationships is provided in Figure 1.

We note that our model does not require state variable boundedness in the description of the dynamics, in contrast to Kvatinsky *et al.* [7], Strukov *et al.* [20]. Instead, we resolve non-physical behavior by the saturation component of the model.

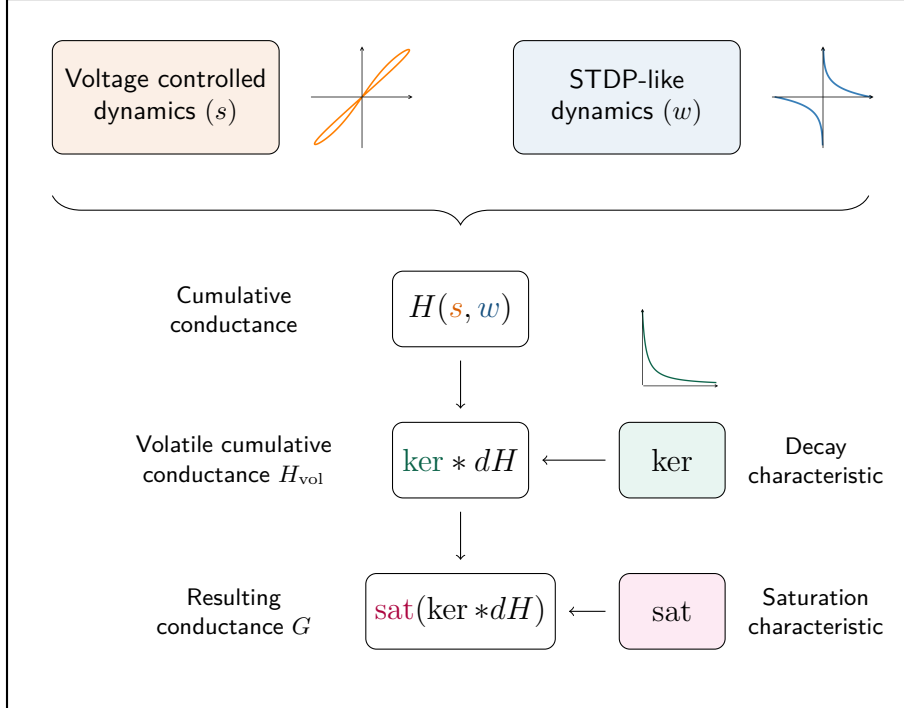


FIG. 1. Schematic representation of the model. The model integrates two independent components into the cumulative conductance function $H(s, w)$: voltage-controlled switching dynamics (state variable s) providing the memristive core, and STDP-like synaptic plasticity (state variable w) implementing learning rules through eligibility traces. The function then undergoes volatile decay through viscoelastic-inspired convolution with a decay kernel $\text{ker}()$. The final conductance G emerges after saturation nonlinearity, reproducing both volatile memory and synaptic plasticity observed in polymeric memristors. This modular approach enables near-independent optimization of each functional component.

A. Voltage-controlled model

We present two voltage-controlled memristor models fitting the general framework for memristive devices suitable as the basis for the non-volatile behavior.

A simple and common [20] possibility is the linear voltage controlled memristor model:

$$\dot{s} = \mu v. \quad (2)$$

A more detailed approach due to [7] is also a popular choice:

$$\dot{s} = \begin{cases} k_{\text{off}} \left(\frac{v(t)}{v_{\text{off}}} - 1 \right)^{\alpha_{\text{off}}}, & \text{if } 0 < v_{\text{off}} < v, \\ 0, & \text{if } v_{\text{on}} < v < v_{\text{off}}, \\ k_{\text{on}} \left(\frac{v(t)}{v_{\text{on}}} - 1 \right)^{\alpha_{\text{on}}}, & \text{if } v < v_{\text{on}} < 0. \end{cases}$$

Notably, we have omitted the windowing functions in the above equations, since in our approach the state parameters are unbounded at this stage of the modeling process. Hence at this stage, the so-called linear memristor model of Eq. (2) is truly a linear differential equation.

It should be emphasized that any kind of voltage-controlled memristor state-variable differential equation in the form specified in Eq. (1) is compatible with our framework.

B. STDP model for a one-port device

In this section, we adapt the local variables synaptic STDP model, as presented in [15], to a one-port physical electronic device, making it compatible with the standard memristive framework. This model provides a phenomenological description of synaptic weight parameter changes based on relative timing of two classes of spiking inputs: presynaptic and postsynaptic. Notably, due to its abstract formulation, the model can be generalized beyond neural systems, provided the two input classes are reinterpreted in an appropriate manner.

To begin, recall the synaptic model's original formulation and interpretation. We consider the synaptic weight variable w , whose dynamics are driven by presynaptic and postsynaptic spike trains S_{pre} and S_{post} , respectively. Denote by (t_f) and (t^n) the presynaptic and postsynaptic spike time sequences. The spike trains are then modeled as a series of Dirac impulses at the corresponding times:

$$S_{\text{pre}}(t) = \sum_f \delta(t - t_f), \quad \text{and} \quad S_{\text{post}}(t) = \sum_n \delta(t - t^n).$$

Define two auxiliary variables x and y , representing the presynaptic and postsynaptic traces, which model the capacity for change in the weight variable w . They are incremented

by their respective spike trains and decay exponentially between spikes:

$$\begin{aligned}\dot{x}(t) &= -\frac{x(t)}{\tau_+} + S_{\text{pre}}(t) \\ \dot{y}(t) &= -\frac{y(t)}{\tau_-} + S_{\text{post}}(t),\end{aligned}$$

where τ_+ , τ_- are time constants.

Finally, the weight variable w is updated at postsynaptic spike times proportionally to the presynaptic trace x , and negatively at postsynaptic spike times in proportion to the postsynaptic trace y :

$$\dot{w}(t) = x(t) A_+(w) S_{\text{post}}(t) - y(t) A_-(w) S_{\text{pre}}(t).$$

The functions A_+ , A_- are weight dependent scaling factors.

Our aim is to reformulate this model for a one-port device, which has important distinctions from biological synapses. The key idea is to replace discrete spike trains with continuous voltage signals, while interpreting one terminal as the 'presynaptic' terminal and the other as the 'postsynaptic' terminal. With this identification, the respective spike trains correspond to positive and negative voltages across the device. Accordingly, we substitute the spike trains at each synaptic terminal with the appropriate signed voltage function, as illustrated below:

$$\begin{aligned}S_{\text{pre}}(t) &\implies v^+(t) \\ S_{\text{post}}(t) &\implies v^-(t),\end{aligned}$$

where v^+ , v^- are the positive and negative parts of v , respectively, with the convention $v = v^+ - v^-$.

By treating the variables w , x , y as additional state parameters of the memristor, we can formulate the STDP model for a one-port device as follows, thereby completing the construction.

$$\begin{aligned}\dot{x} &= -\frac{x}{\tau_+} + v^+ \\ \dot{y} &= -\frac{y}{\tau_-} + v^- \\ \dot{w} &= x A_+(w) v^- - y A_-(w) v^+.\end{aligned}\tag{3}$$

We differ from [15] in our approach by considering unbounded w at this stage. As a result the functions A_+ , A_- do not need to contain a windowing function to force bounds onto the weight parameter.

We note that the exponential decay of the variables x and y is inherited from the synaptic model. However, other volatility dynamics can be considered, for instance by replacing the decay with a more general kernel-based approach. The choice of dynamics determines the shape of the STDP characteristic, in particular the classical double-exponential result is a consequence of the exponential decay for variables x and y .

As a final remark, we note that the full memristive dynamics formulation may incorporate coupling by allowing A_+ and A_- to depend on s .

C. Introducing volatility by analogue with linear viscoelasticity

In order to model memristor volatility characteristics, we implement a standard convolution-based approach, inspired by linear viscoelasticity theory [16]. A key advantage is that this approach enables the use of $1/t^\alpha$ volatility kernels that are otherwise computationally unavailable. Given the functions k and H , denote the Stieltjes convolution as

$$k * dH(t) = \int_{-\infty}^t k(t - \tau) dH(\tau)$$

whenever this Lebesgue-Stieltjes integral is defined[26] In the following, the symbol $*$ will always denote the Stieltjes convolution.

In this approach, we need to select a suitable kernel function $\ker()$, which characterizes the device’s conductance volatility, and the *cumulative conductance function* $H(s, w)$, which describes nonvolatile behavior of conductance. The resulting *volatile cumulative conductance* H_{vol} is calculated as the convolution

$$H_{\text{vol}} = \ker * dH(s, w). \quad (4)$$

Note that the convolution is calculated with respect to time, since the model state variables s and w are time-dependent. Similarly, the differential dH must also be taken with respect to time, written explicitly[27]:

$$dH = \partial_s H(s, w) \dot{s} + \partial_w H(s, w) \dot{w}. \quad (5)$$

Regarding the kernel function, we may distinguish two cases, based on its limiting behavior. For example, if the kernel is the Heaviside function, no volatile behavior is present (pure “elastic” regime), and Eq. (4) simplifies to

$$H_{\text{vol}} = H(s, w).$$

This relation motivates the label "cumulative conductance" for the function H ; it captures the functional relationship of state variables and device conductance in the non-volatile case. Conversely, if $\lim_{t \rightarrow \infty} \ker(t) = 0$, we are in the viscoelastic regime, where the system decays to its equilibrium over time.

Our model is therefore sufficiently general to describe devices exhibiting a combination of volatile and non-volatile characteristics.

The form of the kernel and cumulative conductance functions is device-specific and also depends on the chosen voltage-controlled model in Section II A. Inspired by the presentation in Kvatinsky *et al.* [7], we provide ad-hoc variants for the kernel function and for the cumulative conductance function.

First, a linear and exponential relationship of the cumulative conductance on the state variables are presented:

$$\begin{aligned} dH(s, w) &= h_1 \dot{s} + h_0 \dot{w} \\ dH(s, w) &= h_1 e^{as} \dot{s} + h_0 e^{bw} \dot{w}. \end{aligned}$$

The terminology corresponds to the relationships in the case of the purely elastic regime ($\ker()$ is the Heaviside function), as discussed above. These two versions are generalizations of the current-voltage relationships presented in Kvatinsky *et al.* [7].

Similarly, one can consider variants for the kernel:

$$\begin{aligned} \ker(t) &= e^{-at} \\ \ker(t) &= \frac{1}{(t + \varepsilon)^a}, \end{aligned}$$

for $t > 0$ and identically zero for negative times. The power-law kernel may be offset by a small positive ε to avoid the singularity at zero.

In addition, we offer a rigorous but data-specific approach for deriving the functional forms of the volatility characteristics $\ker()$ and H in Section IV A and Section IV C, respectively. We do so using data from pulse stimulation of the device, idealized by a single box function. Consequently, in Section IV D we consider a conductance function of the form

$$dH(s, w) = (h_{11} |s|^a + h_{10})\dot{s} + (h_{01}|w|^a + h_{00})\dot{w}. \quad (6)$$

D. Introducing saturation via linear-nonlinear approach

Since the approach described so far allows memristor conductance values that are unbounded and could even become negative, it is necessary to limit the conductance to realistic bounds. To obtain the resulting conductance from the volatile, unbounded version Eq. (4), we employ the linear-nonlinear scheme [15]; a standard method to introduce nonlinearities, such as saturation, into a linear system.

Hence, we calculate the resulting conductance G as:

$$G = \text{sat}(H_{\text{vol}}), \quad (7)$$

where $\text{sat}()$ is a chosen nonlinear saturation function.

Sigmoid functions are a common choice for saturation functions given their flexibility, hence here we adopt the logistic function:

$$\text{sat}(h) = (g_{\max} - g_{\min}) \frac{1}{1 + e^{-Ah}} + g_{\min}, \quad (8)$$

where

$$A = \frac{4}{h_{\max} - h_{\min}}$$

to best align the linear portion of the logistic function with the range of conductance.

E. Complete model of volatile memristor with STDP

Combining the results of sections II A – II D we formulate the complete model.

1. Consider the vector (s, w, x, y) of state parameters and define the dynamics of the state variables by choosing an equation for s from section II A, and Eq. (3) for x, y, w .
2. Next, as per section II C choose an appropriate kernel function $\text{ker}()$ and cumulative conductance function H and calculate its derivative.
3. Compute the volatile pre-conductance H_{vol} by Eq. (4).
4. The resulting conductance $G(t)$ is obtained from Eq. (7).

III. EXPERIMENTAL DATA

The proposed model is validated against experimental data obtained from polymeric memristive devices that were synthesised and experimentally characterized by Panthi *et al.* [22]. In low voltage regime, these devices exhibit a rich set of synaptic-like behaviors, including history-dependent conductance changes and volatile memory, which provide the experimental grounding for our model’s structure.

A. Polymeric memristor with neuro-synaptic properties

The experimental validation of our model employs memristive devices based on poly[N-(3-(9H-carbazol-9-yl)propyl)methacrylamide] (PCaPMA). In these devices, a thin PCaPMA film is sandwiched between an indium tin oxide (ITO) bottom electrode and a top electrode made of Au or Al. The resulting structure functions as a two-terminal memristive element whose conductance depends on the history of applied voltage pulses.

Panthi *et al.* demonstrated that such PCaPMA devices can emulate a broad repertoire of synaptic functions that are central for neuromorphic computing [22]. When excited by trains of low-amplitude voltage pulses, the device conductance can be gradually increased (potentiation) or decreased (depression), depending on the polarity, number, amplitude, and frequency of the pulses. The same platform supports both short- and long-term plasticity, paired-pulse facilitation and depression (PPF/D), spike-timing dependent plasticity (STDP), and simple associative learning protocols, all on millisecond timescales. These characteristics make the PCaPMA memristor a natural candidate for validating compact models that aim to unify memristive switching, volatility, and synaptic plasticity.

The microscopic origin of the resistive switching in PCaPMA has been attributed to a combination of voltage-induced conformational changes of the polymer, trapping and detrapping of charge carriers at localized sites, and redox phenomena within the active layer [21, 22]. A detailed microscopic description of these intertwined processes is beyond the scope of the present work; instead, we treat them as defining an effective internal state whose dynamics is captured phenomenologically by the state variables of our model and by the cumulative conductance function $H(s, w)$.

Beyond the synaptic functions reported in Panthi *et al.* [22], our collaboration with

the device-fabrication team provided access to extensive relaxation and timing datasets obtained on the same class of devices, including unpublished measurements. These data show that, after potentiation by a finite pulse train, the conductance relaxes slowly over several decades in time, with decay curves that are close to linear when plotted in double-logarithmic coordinates (Figure 3). This long-tailed relaxation is inconsistent with a single exponential and forms the empirical basis for our choice of a power-law-like memory kernel in the volatility module.

For modeling purposes, the key device-level properties that we retain from the PCaPMA system are therefore: (i) analog, gradual conductance modulation by trains of voltage pulses; (ii) coexistence of volatile and non-volatile plasticity on millisecond–second timescales; and (iii) low-voltage operation compatible with mixed-signal neuromorphic circuits. While our framework is formally material-agnostic, PCaPMA provides a concrete polymer platform whose experimentally characterized synaptic-like behavior and volatile relaxation impose quantitative constraints on the kernel $\ker(t)$, the cumulative conductance $H(s, w)$, and the saturation module.

IV. FITTING MODEL TO EXPERIMENTAL DATA

Application of our model to experiments relies on comprehensive electrical characterization data, using protocols designed to isolate different aspects of memristive behavior. Measurements were done using trains of stimulation pulses (± 500 mV, 20 ms duration) with interleaved read pulses (-50 mV, 50 ms duration) to monitor conductance evolution. Owing to observed voltage-threshold behavior, the contribution of the read pulses was considered negligible and therefore omitted from the model simulations.

Two measurement protocols formed the empirical basis for model development. First, relaxation measurements following stimulation at different intensities revealed volatile memory dynamics, with conductance monitored over timescales from tens of milliseconds to hundreds of seconds. Second, specialized timing protocols captured STDP characteristics by varying the delay between paired pulses, mapping the full spectrum of causal and anti-causal plasticity.

To derive the model for a given device, we first extract the characteristic volatility kernel from the relaxation measurements using an approximation technique. We then apply the Laplace method described in IV C to determine the form of the cumulative function and

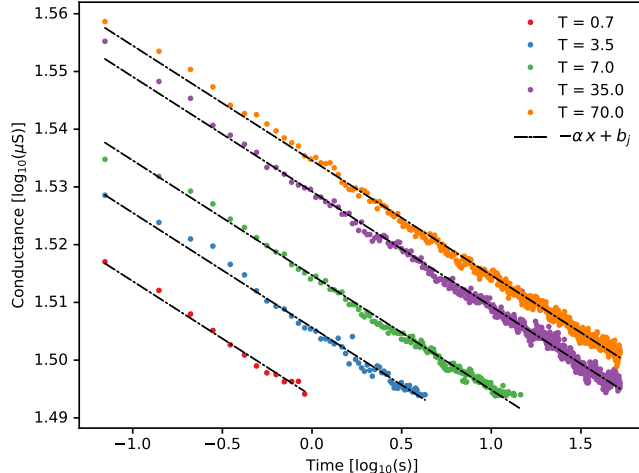


FIG. 2. Log–log representation of post-potiation conductance relaxation in the PCaPMA memristor. Each curve shows the decay of conductance after a train of trigger pulses with different total stimulation time T_j . When plotted in double-logarithmic coordinates, the initial segments of all traces are close to straight lines over more than two decades in time, indicating a power-law-like decay and ruling out a simple exponential relaxation.

estimate the corresponding parameters. Next, we estimate the parameters of the STDP module from measurements and finally set the saturation module coefficients either to minimally affect the model, or by performing a joint optimization of all parameters.

A. Determining the kernel-function form

In this section we derive the functional form of the kernel from conductance relaxation measurements. The decay segments of the conductance evolution are shown in log-log coordinates in Figure 2, with data that deviate from the linear behavior omitted. It is visible that the initial slopes of the decay are linear up to over two orders of magnitude, which excludes exponential decay. We fit the data using functions of the form $-\alpha x + b_j$, where α is the common slope and b_j is the individual offset.

The function $-\alpha x + b$ is transformed into lin-lin coordinates as

$$\bar{b} \frac{1}{x^\alpha},$$

for a suitably modified \bar{b} . The expression is undefined for $x = 0$, so a small positive shift by ε is introduced. The addition of ε preserves the short-time characteristic of the relaxation,

but avoids the singularity at zero.

Owing to the power-law characteristic, we are considering the kernel function in the form

$$\ker(t) = \begin{cases} 0, & \text{if } t < 0 \\ \frac{1}{(t + \varepsilon)^{\alpha+1}}, & \text{if } t \geq 0, \end{cases} \quad (9)$$

for $\alpha > 0$. To ensure proper scaling, the kernel must be normalized. To this end set

$$I_\varepsilon = \int_\varepsilon^\infty \frac{1}{x^{\alpha+1}} dx = \frac{1}{\alpha \cdot \varepsilon^\alpha},$$

and define the resulting normalized kernel as

$$\frac{\ker(t)}{I_\varepsilon}.$$

B. Finding the kernel-function coefficient α

To estimate the value of α that results in the measured conductance G , assume the conductance data are the response to a box function of applied voltage $b \chi_{(-T,0)}$, where b is a scalar and T is the time of applied stimulation.

$$G(t) = b \chi_{(-T,0)} * \ker(t) + c,$$

for a suitable stationary conductance constant c . We calculate

$$\begin{aligned} G(t) &= b \int_{-\infty}^t \ker(t - \tau) \chi_{(-T,0)}(\tau) d\tau + c = b \int_{-T}^0 \ker(t - \tau) d\tau + c \\ &= b \int_t^{T+t} \ker(u) du + g_0 = b (K(t+T) - K(t)) + c \end{aligned}$$

where

$$K(t) = \int_{-\infty}^t \ker(\tau) d\tau = \begin{cases} 0, & \text{if } t < 0 \\ 1 - \frac{\varepsilon^\alpha}{(t + \varepsilon)^\alpha}, & \text{if } t \geq 0, \end{cases}$$

is a primitive function to $\ker()$. To derive the decay characteristic after the pulse stimulation from time $-T$ to 0, fit the decay of the graph to the function for $t \geq 0$

$$G(t) = b (K(t+T) - K(t)) + c = b \left(\frac{\varepsilon^\alpha}{(t + \varepsilon)^\alpha} - \frac{\varepsilon^\alpha}{(t + T + \varepsilon)^\alpha} \right) + c$$

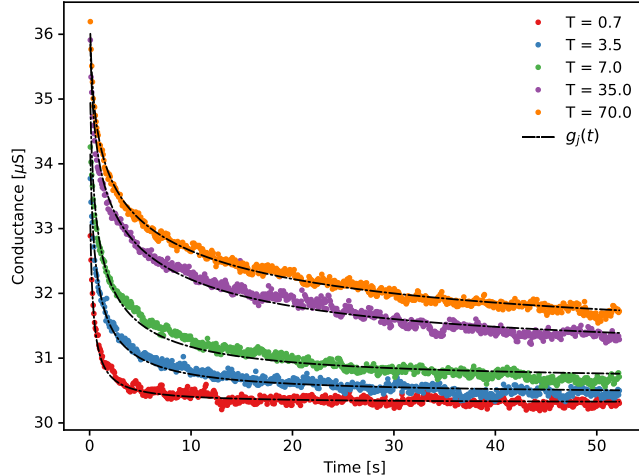


FIG. 3. Kernel function coefficient estimation. Each trace corresponds to stimulation by pulses over the duration T_j . For each trace, a fit $g_j(t) = b_j \left(\frac{1}{(x+\varepsilon)^\alpha} - \frac{1}{(x+\varepsilon+T_j)^\alpha} \right) + c_j$ is performed using two trace-specific parameters b_j and c_j together with the global coefficient α to be estimated.

We repeat the above procedure for every measured trace and find an optimal α over all six datasets, as shown in Figure 3.

We have set ε to the time resolution of the measurements (70ms) and calculated the value of alpha to be $\alpha = 0.029$, which corresponds to the volatility following a power-law with an exponent 1.029.

C. Derivation of cumulative conductance

In this section we describe a method for determining the form of the cumulative conductance function H . We do so using data from pulse stimulation, again idealized by a single box function similarly as in Section IV B. The procedure yields only the dependence on the parameter s , the dependence on w must be copied, or derived in a different way.

Our goal is to find the cumulative conductance function such that the prediction given by the model results in the traces g_j from Figure 3. Note that because the following utilizes the Laplace transform, we must restrict ourselves to positive times, hence in contrast to the discussion in Section IV B we work with the single box function supported on the interval $(0, T)$, i.e. $\chi_{(0,T)}$.

1. We use the previously calculated traces dependent on T_j :

$$g_j = b_j \ker * \chi_{(0,T)} + c_j .$$

2. Find explicit functions $b(T)$ and $c(T)$ that describe the dependence of b_j and c_j on T_j , respectively. In our case, we find by minimization appropriate constants b^i, c^i such that

$$\begin{aligned} b(T) &= b^1 \log(T + b^2) + b^3 \\ c(T) &= c^1 \log(T + c^2) + c^3 . \end{aligned}$$

Then the traces become

$$g = b(T) \ker * \chi_{(0,T)} + c(T) . \quad (10)$$

3. Neglecting the saturation term, our model predicts $g = \ker * dH(s) + g_0$, where $dH(s(t)) = \partial_s H(s(t)) \dot{s}(t)$. Recall the voltage-control linear differential equation Eq. (2), $\dot{s} = \mu v$, and consider a normalized voltage input $v = \chi_{(0,T)}$. Then it holds that $s(t) = \mu t$ and by setting Eq. (10) equal to our model we obtain:

$$\ker * (\partial_s H(s) \mu \chi_{(0,T)}) + g_0 = b(T) \ker * \chi_{(0,T)} + c(T) .$$

4. We apply the Laplace transformation to both sides and perform some rearranging to derive the form of dH , valid for $t \in [0, T]$:

$$\begin{aligned} \mathcal{L}(\ker) \mathcal{L}(\partial_s H(s) \mu \chi_{(0,T)}) + \frac{1}{s} g_0 &= b(T) \mathcal{L}(\ker) \mathcal{L}(\chi_{(0,T)}) + \frac{1}{s} c(T) \\ \mu \partial_s H(\mu t) &= \mathcal{L}^{-1} \left\{ \left(b(T) \mathcal{L}(\ker) \mathcal{L}(\chi_{(0,T)}) + \frac{1}{s} (c(T) - g_0) \right) / \mathcal{L}(\ker) \right\} . \end{aligned}$$

5. In our case, the calculation of the Laplace transform of $\ker()$ and $\chi_{(0,T)}$ is performed, up to normalization constant, as

$$\begin{aligned} \mathcal{L}(\ker)(s) &= s^\alpha e^{s\varepsilon} \Gamma(\alpha, s\varepsilon) \\ \mathcal{L}(\chi_{(0,T)})(s) &= \frac{1}{s} (1 - e^{-sT}) , \end{aligned}$$

where $\Gamma(a, x) = \int_x^\infty t^{a-1} e^{-t} dt$ is the upper incomplete Gamma function.

As a result, the above procedure yields the following expression for positive values of x :

$$\partial_s H(x) = h_1 x^\alpha + h_0 .$$

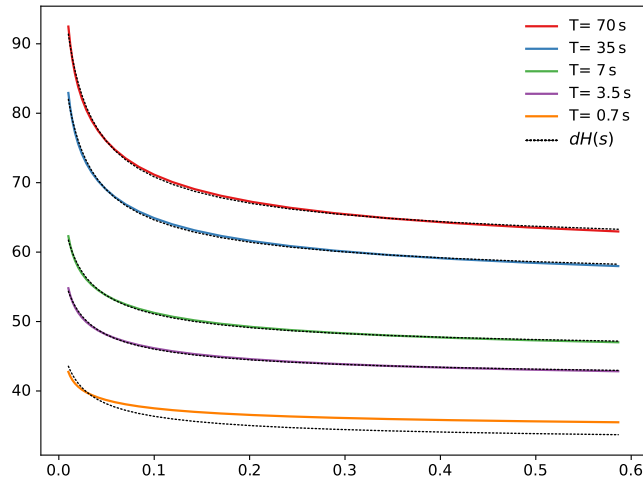


FIG. 4. Cumulative conductance function estimate. Each curve shows the estimated dependence of $\partial_s H(s)$ on the state variable s , reconstructed from relaxation traces with different stimulation durations T using the procedure in IV C. The parameters h_0 , h_1 are chosen so that the traces for all T collapse onto a power-law-like curve with a common $a = -0.585$, well approximated by the parametric form $dH(s) = (h_1 |s|^a + h_0) \dot{s}$. This justifies the simple functional form of dH used in the main text.

In general there may be some dependence of H on T (refer to Figure 4), and we choose the parameters h_1 , h_0 of the cumulative function that minimizes such dependence. To obtain dH , extend the relationship symmetrically for $x < 0$, hence the resulting functional form is

$$dH(s) = (h_1 |s|^a + h_0) \dot{s} \quad (11)$$

D. Finding cumulative conductance function coefficients

Having determined the characteristic of the decay, we now turn to estimating the parameters for the remaining parts of the model. Neglecting the saturation component for now, the resulting conductance G is predicted by the model as:

$$G = \ker * dH + g_0.$$

We are considering dH in the form derived in IV C:

$$dH(s) = (h_1 |s|^a + h_0) \dot{s},$$

where we already have estimated the optimal coefficient $a = -0.585$, and are looking to estimate the parameters h_0 and h_1 . For demonstration, we perform the fit on the stimulation segment of the traces above, this time with the precise input data. We obtain the graphs in Figure 5.

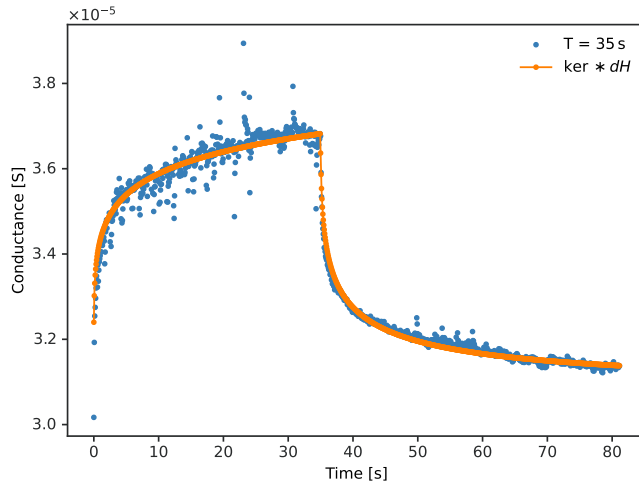


FIG. 5. Comparison between the model and the experimental data for a relatively long stimulation input ($T = 35$ s). The measured conductance decays after potentiation by a pulse train of total duration T and the solid line shows the corresponding numerical simulation of the model.

E. Modeling STDP

To estimate the coefficients of the STDP component, we extend the previously computed part of the model with the dependence on the weight parameter w . Specifically we are now looking to estimate the coefficients from Eq. (3): A_+ , A_- , τ_+ , τ_- , as well as the coefficients from the STDP component of dH ; h_{01} and h_{00} .

The data under evaluation consists of three conductance measurements per run. The first determines the steady-state conductance g_0 , while the other two quantify the the conductance change ΔG : one measured 10ms after the end of the second testing pulse (denoted t_1) and another measured after 100ms (denoted t_2). We optimize the parameters for the first measurement, since the second one should be a result of the volatility modeled by $\ker()$.

It should be noted, that this estimate is considered to independent of the previous discussion, since any effect arising from the variable s is effectively canceled out by the use of equal but opposite pulses in these measurements and simulations.

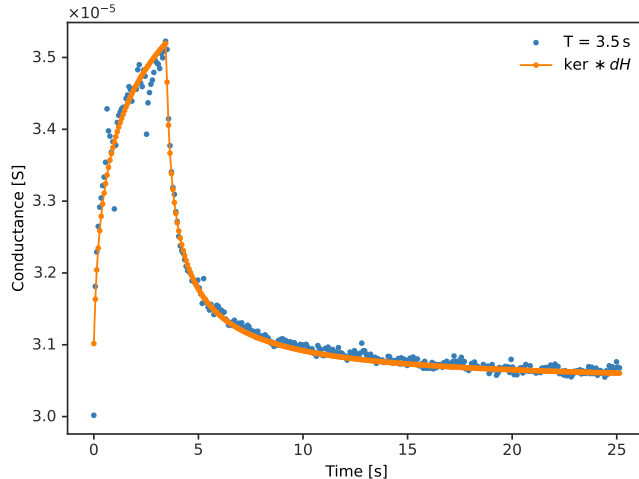


FIG. 6. Comparison between experimental relaxation and model prediction for a shorter stimulation train ($T = 3.5$ s). As in Figure 2, the dots show the measured post-potential conductance decay and the solid line the prediction of the same volatility kernel Eq. (9) and cumulative conductance function $H(s)$ as in fig. 5. The overall good agreement across the entire decay window indicates that a single, material-specific kernel captures the volatile dynamics for different stimulation protocols.

We calculate the difference in resting and STDP-induced conductance

$$\Delta G = \frac{\text{ker} * dH(t_1) - g_0}{g_0},$$

and estimate the parameters of the model to fit the measurements. The results of the STDP-induced conductance at both sample times are shown in fig. 7. As a consequence, we verified that the decrease in STDP effects over time is a result of the previously modeled volatility mechanism.

F. Implementing saturation

Up to now, we have ignored the effects of saturation in the modeling for simplicity of presentation. We thus implicitly assumed the effects modeled so far lie in the linear regime of the saturation curve, so that the subsequent addition of the saturation component will have minimal effect.

The above discussed approach may be repeated with chosen coefficients for the saturation module to obtain optimized model parameters that now include the effects of saturation. Suitable coefficients for g_{\max} , g_{\min} , h_{\max} and h_{\min} are presented in A.

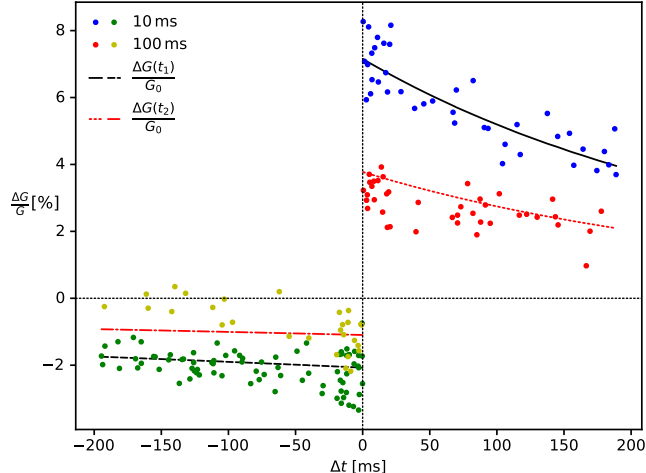


FIG. 7. Fit and prediction of the STDP-like behavior. The dots show the experimentally measured relative conductance changes $\Delta G/G_0$ as a function of spike-timing difference Δt for a paired-pulse protocol applied to the PCaPMA memristor. The black lines represent the model output with parameter values fitted to the data at reading delay $t_1 = 10$ ms. The red lines represent the prediction of the model, with the same parameters, when evaluated at reading delay $t_2 = 100$ ms.

V. DISCUSSION

We have introduced a modular memristor model that unifies a voltage-controlled memristive core, synaptic-like plasticity and volatile relaxation within a single, computationally efficient framework. By grounding the modules for volatility and plasticity in principles from condensed matter physics and computational neuroscience, respectively, the model moves beyond pure phenomenology to provide a physically and biologically plausible description of complex memristive behaviors.

A. Extending the state-of-the-art memristor models

The current landscape of compact memristor modeling is dominated by frameworks such as the TEAM and VTEAM models, which provide computationally efficient descriptions of the core resistive switching but are fundamentally phenomenological [6, 7]. Other approaches have examined the dynamical aspects of memristive switching, including shock-wave propagation phenomena that govern commutation speed [28]. Our model extends this state-of-the-art by incorporating two crucial, biologically inspired features—synaptic plasticity and volatile

memory—not as ad-hoc additions, but as modules derived from established theoretical principles.

In neuromorphic contexts, the STDP module enables biologically plausible learning rules, facilitating simulations of associative memory and adaptation [5, 13, 14].

To model synaptic plasticity, we implement a spike-timing-dependent plasticity (STDP) rule inspired by the work of Gerstner *et al.* [15]. This approach is based on the concept of eligibility traces, a cornerstone of modern theories of learning in the brain. In this framework, plasticity is a two-stage process. First, the near-coincidence of pre- and post-synaptic activity creates a short-lived synaptic "tag" or trace that marks the synapse as "eligible" for modification. Second, this temporary trace is only converted into a lasting weight change if a third, modulatory signal—representing global factors like reward, novelty, or surprise—arrives while the trace is still active [29]. By adopting this mechanism, our model moves beyond simple pairwise STDP to support more powerful and flexible three-factor learning rules. This capability aligns the model with cutting-edge research in reinforcement learning and makes it a compelling component for building truly adaptive neuromorphic systems.

To model memory volatility, we took inspiration from the theory of linear viscoelasticity, which describes history-dependent phenomena in materials science [17]. The mathematical structure is that of a hereditary integral, where the current conductance state is a convolution of the entire past history of voltage stimuli with a decaying memory kernel. On top of this linear convolution, we add a final nonlinearity to shape the output conductance. This structure is analogous to the well-known linear-nonlinear models widely used in computational neuroscience to describe the relationship between a stimulus and a neuron's firing rate [15]. In our model, the linear filter captures the device's history-dependent memory, while the subsequent nonlinear stage accounts for saturation and other device-specific characteristics.

In contrast to the V-VTEAM model [9], which implements a stretched-exponential volatility model directly in the formulation of the dynamics, our approach to volatility is threshold independent and offers a broad range of possible decay characteristics. For example, a differential equation formulation for a $1/t$ kernel is notoriously computationally unstable, but poses no difficulty in the convolution approach.

B. Physical origin of the 1/t-like memory kernel

As shown in Section IV B, the volatility module of our model is governed by the hereditary kernel in Eq. (9) with an exponent $\alpha \approx 0.03$ obtained from the log–log relaxation data in Figure 2. The corresponding cumulative memory $K(t) = \int_{-\infty}^t \ker(\tau) d\tau$ decays approximately as $K(t) \sim 1/t$ for large t . In practice, the device therefore exhibits effectively 1/t-like “loss of memory” over time.

Power-law relaxations of this type are typical for transport in disordered media. In a broad class of disordered conductors, charge transport proceeds along percolating networks of microscopic pathways, and charge carriers perform a continuous-time random walk (CTRW) with a broad distribution of waiting times between hops [18, 30, 31]. If the waiting-time distribution $\psi(\tau)$ has a heavy tail, e.g. $\psi(\tau) \sim \tau^{-1-\alpha}$ with $0 < \alpha < 1$, the resulting transport is sub-diffusive and the macroscopic response to a perturbation relaxes as a power law rather than as a sum of exponentials. In our context, the “response” is the conductance of the memristive device following a potentiating pulse train, and the observed long-tailed decay directly motivates the 1/t-like kernel in Eq. (9).

The viscoelastic analogy used in Section II A provides a convenient heuristic explanation of this situation. In linear viscoelasticity, a material with a broad spectrum of relaxation times $\rho(\tau)$ can be represented as a superposition of many Maxwell modes, and a spectrum $\rho(\tau) \propto \tau^{-1-\alpha}$ yields an effective relaxation modulus $G(t) \propto t^{-\alpha}$ [17, 19]. Our choice of $\ker(t) \propto (t + \varepsilon)^{-(\alpha+1)}$ plays the same role: it compactly encodes the presence of many internal relaxation processes without having to resolve them individually at the level of the model.

For the PCaPMA devices used here, the microscopic origin of such a broad relaxation spectrum is likely associated with structural and energetic disorder in the polymer, together with charge trapping/detrapping and redox processes in the active layer, as discussed in Panthi *et al.* [22]. Different local environments and slow morphological rearrangements would naturally generate a hierarchy of timescales. Our model does not attempt to distinguish these mechanisms explicitly. Instead, the 1/t-like kernel should be viewed as a phenomenological summary of their cumulative effect, constrained by the experimentally observed long-tailed relaxation in Figures 2 and 3.

Importantly, the argument leading to a power-law kernel is not specific to PCaPMA. Percolation-controlled transport and CTRW-style dynamics are common in organic and

hybrid memristive systems [12]. We therefore expect that, when adapting the present framework to other polymeric or soft-matter memristors, only the kernel exponent α and an overall time scale need to be adjusted, while the basic structure of the volatility module – a viscoelastic-type kernel acting on the cumulative conductance function $H(s, w)$ – remains unchanged.

C. Adapting model to polymeric memristor

PCaPMA combines processability (solution casting/printing), morphological stability (nm-scale roughness)[21], and low-voltage operation with rich neurosynaptic functionality [22]. Evidence from transport and spectroscopy points to a multi-mechanism picture in which conformational reorientation of carbazole side groups, trapping/detrapping at localized states, interfacial barrier modulation, and redox processes jointly modulate conductance; critically, repeated pulsing produces analog, history-dependent updates consistent with synaptic potentiation/depression at $\pm(0.3\text{--}0.6)$ V and 5–20 ms widths. Spike-rate dependence reveals an STP→LTP transition with repetition rate (> 1 Hz), and paired-pulse and STDP protocols yield causal/anti-causal weight changes with time constants in the $\mathcal{O}(10^2)$ ms range, compatible with our local-trace plasticity module [15, 22].

D. Prospective model extensions

The modularity of the proposed model is one of its key strengths and opens several avenues for future work. Each component—the non-volatile core, the volatility kernel, and the plasticity rule—can be modified or replaced independently to adapt the model to different physical devices or to explore alternative theoretical assumptions. This allows for the separate experimental characterization and fitting of each module, simplifying the process of model validation and refinement for new memristive technologies.

Furthermore, while the current model is deterministic, the experimental data clearly exhibit stochasticity. This inherent randomness in polymeric devices is not necessarily a flaw; it can be a functional feature. For example, recent work has demonstrated that the stochastic switching of polymeric memristors can be used as a physical entropy source for applications in probabilistic computing [32]. A natural extension of our work would be to incorporate a

stochastic component into the model, which would not only improve its descriptive accuracy but also allow it to be used for designing and simulating such novel computing paradigms.

The $1/t$ form is phenomenological; multiple microscopic routes (trapping/detrapping spectra, filament reconfiguration, ionic drift) can lead to similar envelopes. Future work should correlate α with material properties (electrode, thickness, processing) and examine frequency dependence.

VI. CONCLUSIONS

We have presented a modular and computationally efficient compact model for memristors that exhibits both volatile memory and synaptic-like plasticity. The model’s key innovation lies in the synthesis of several modeling techniques that allow for memristor current-voltage characteristics, synaptic-like plasticity effects and a general description of relaxation dynamics (volatile memristor memory) with saturation. We have discussed how the volatile relaxation dynamics, experimentally observed as a power-law decay, can be described by a viscoelasticity-inspired hereditary integral whose form is physically justified by percolation theory. Furthermore, we have demonstrated that a biologically plausible model of STDP based on eligibility traces can be implemented, endowing the future devices with a potential capacity for advanced learning.

The complete model was shown to be in excellent quantitative agreement with experimental data from polymeric memristors. However, we believe that the modularity and relative simplicity of the proposed model allow its implementation (including validation) in a wide range of memristive-like devices. Therefore, this work provides a unified, mathematically grounded framework for understanding and simulating complex memristive devices, offering a valuable tool for advancing the design of neuromorphic computing systems.

ACKNOWLEDGMENTS

This work was supported by The Czech Science Foundation project No. 24-10384S, MEYS project Inter-Excellence No. LUAUS24032 and the Strategy AV 21 Programme “Breakthrough Technologies for the Future – Sensing, Digitisation, Artificial Intelligence, and Quantum Technologies”.

$$\alpha 0.029$$

TABLE I. Volatility power law coefficient estimate.

D.H. and L.K. conceived and led the project, carried out the theoretical development, implemented the model and simulations, analyzed the data, and wrote the manuscript. S.H.F. and K.K. contributed to the theoretical development and provided critical feedback and revisions to specific sections of the manuscript. A.P., Y.R.P., J.P., and J.V. fabricated the polymeric memristors and performed the experimental measurements. All authors reviewed the manuscript and approved the final version.

Data availability

The source data of PPF/PPD and STDP can be accessed from Zenodo at <https://zenodo.org/records/12685756>.

Appendix A: Numerical values

Here we collect numerical values of the parameters fitted in the preceding sections. They are not required for understanding the structure of the model, but they provide a complete description of the specific PCaPMA device and protocols used in our study.

The first table I lists the kernel exponent α obtained from the analysis presented in Section IV B. The second table II summarizes the amplitudes b and offsets c of the relaxation traces for each stimulation duration T , which determine the functions $b(T)$ and $c(T)$ appearing in the cumulative conductance function-reconstruction procedure of IV C. The cumulative conductance function power law coefficient is shown in Table III. The table IV lists cumulative conductance coefficients h_1 and h_2 , as well as model coefficients μ and g_0 , estimated to fit the potentiation segment of Figure 5 and Figure 6.

Table V reports the parameters of the STDP module (Section II B and Eq. (3)), which are used to generate the model STDP curve in Figure 7. Our choice for the parameters of the saturation module are presented in table VI

Together, these values define a reproducible parameter set for the particular device studied,

T	70	35	7	3.5	0.7
b	54.65	41.44	40.23	33.07	29.78
c	30.31	30.43	30.63	30.98	31.13

TABLE II. Numerical values of the trace-specific amplitudes b and offsets c obtained from fitting the relaxation traces for different stimulation durations T (cf. IV B). These values determine the functions $b(T)$ and $c(T)$ in Eq. (10), which are used to derive the kernel function $\ker(t)$ and, in turn, the form of the cumulative conductance function $H(s)$ from the experimental data.

a	-0.585
-----	--------

TABLE III. Cumulative conductance function power law coefficient estimate.

while keeping the main text focused on the general modeling framework.

-
- [1] J. J. Yang, D. B. Strukov, and D. R. Stewart, Memristive devices for computing, *Nat. Nanotechnol.* **8**, 13 (2013).
 - [2] D. Ielmini and H.-S. P. Wong, In-memory computing with resistive switching devices, *Nat. Electron.* **1**, 333 (2018).
 - [3] L. O. Chua, Memristor—the missing circuit element, *IEEE Trans. Circuit Theory* **18**, 507 (1971).
 - [4] L. O. Chua and S.-M. Kang, Memristive devices and systems, *Proc. IEEE* **64**, 209 (1976).
 - [5] S. H. Jo, T. Chang, I. Ebong, B. B. Bhadviya, P. Mazumder, and W. Lu, Nanoscale memristor device as synapse in neuromorphic systems, *Nano Lett.* **10**, 1297 (2010).

T	h_{11}	h_{10}	μ	g_0
3.5 s	1.70×10^{-6}	44.8×10^{-6}	0.226	3.07×10^{-5}
35 s	2.78×10^{-6}	54.4×10^{-6}	0.215	3.08×10^{-5}

TABLE IV. Estimate of model parameters. Owing to the stochastic nature of the polymer-based memristor under study, we obtain a good fit per measured trace of potentiation stimulation.

a_+	10.9
a_-	0.90
τ_+	0.176
τ_-	0.619
h_{01}	1.01×10^{-4}
h_{00}	2.52×10^{-3}

TABLE V. Numerical values of the parameters of the STDP module used in Section IV E. The parameters a_+ , a_- and τ_+ , τ_- define the shapes and time constants of the potentiating and depressing lobes in the local-variable STDP dynamics Eq. (3), the coefficients h_{01} and h_{00} determine the dependence of the cumulative conductance function H on the variable w as in Eq. (6). These values are used to generate the model STDP curve shown in Figure 7 and to ensure consistency between the dynamical STDP formulation and the measured memristor response.

g_{\max}	5×10^{-5}
g_{\min}	1.17×10^{-5}

TABLE VI. The saturation module coefficients were chosen to minimize the effect of added saturation to the model. The parameters h_{\max} , h_{\min} were set equal to g_{\max} , g_{\min} , respectively.

- [6] S. Kvatinsky, E. G. Friedman, A. Kolodny, and U. C. Weiser, TEAM: Threshold adaptive memristor model, *IEEE Trans. Circuits Syst. I* **60**, 211 (2013).
- [7] S. Kvatinsky, N. Ramadan, E. G. Friedman, and A. Kolodny, VTEAM: A general model for voltage-controlled memristors, *IEEE Trans. Circuits Syst. II* **62**, 786 (2015).
- [8] S. Wu, X. Luo, S. Turner, H. Peng, W. Lin, J. Ding, A. David, B. Wang, G. Van Tendeloo, J. Wang, and T. Wu, Nonvolatile resistive switching in pt/laalo3/srtio3 heterostructures, *Phys. Rev. X* **3**, 041027 (2013).
- [9] T. Patni, R. Daniels, and S. Kvatinsky, V-vteam: A compact behavioral model for volatile memristors, in *2024 IEEE International Flexible Electronics Technology Conference (IFETC)* (2024) pp. 1–4.
- [10] Z. Wang, S. Joshi, S. E. Savel'ev, H. Jiang, R. Midya, P. Lin, M. Hu, N. Ge, J. P. Strachan, Z. Li, Q. Wu, M. Barnell, G.-L. Li, H. L. Xin, R. S. Williams, Q. Xia, and J. J. Yang, Memristors with diffusive dynamics as synaptic emulators for neuromorphic computing, *Nat.*

- Mater. **16**, 101 (2017).
- [11] D. Kim, B. Jeon, Y. Lee, D. Kim, Y. Cho, and S. Kim, Prospects and applications of volatile memristors, *Appl. Phys. Lett.* **121**, 010501 (2022).
- [12] R. Wang, J.-Q. Yang, J.-Y. Mao, Z.-P. Wang, S. Wu, M. Zhou, T. Chen, Y. Zhou, and S.-T. Han, Recent advances of volatile memristors: Devices, mechanisms, and applications, *Adv. Intell. Syst.* **2**, 2000055 (2020).
- [13] C. Zamarreño-Ramos, L. A. Camuñas-Mesa, J. A. Pérez-Carrasco, T. Masquelier, T. Serrano-Gotarredona, and B. Linares-Barranco, On spike-timing-dependent-plasticity, memristive devices, and building a self-learning visual cortex, *Front. Neurosci.* **5**, 26 (2011).
- [14] T. Serrano-Gotarredona, T. Masquelier, T. Prodromakis, G. Indiveri, and B. Linares-Barranco, Stdp and stdp variations with memristors for spiking neuromorphic learning systems, *Front. Neurosci.* **7**, 2 (2013).
- [15] W. Gerstner, W. M. Kistler, R. Naud, and L. Paninski, *Neuronal Dynamics: From Single Neurons to Networks and Models of Cognition* (Cambridge University Press, 2014).
- [16] B. D. Coleman and W. Noll, Foundations of linear viscoelasticity, *Rev. Mod. Phys.* **33**, 239 (1961).
- [17] R. G. Larson, *The structure and rheology of complex fluids* (Oxford University Press, 1999).
- [18] D. Stauffer and A. Aharony, *Introduction to Percolation Theory* (Taylor & Francis, 1994).
- [19] J. Song, N. Holten-Andersen, and G. H. McKinley, Non-maxwellian viscoelastic stress relaxations in soft matter, *Soft Matter* **19**, 7885 (2023).
- [20] D. B. Strukov, G. S. Snider, D. R. Stewart, and R. S. Williams, The missing memristor found, *Nature* **453**, 80 (2008).
- [21] Y. R. Panthi, J. Pflieger, D. Výprachtický, A. Pandey, M. A. Thottappali, I. Šeděnková, M. Konefał, and S. H. Foulger, Rewritable resistive memory effect in poly[n-(3-(9h-carbazol-9-yl)propyl)-methacrylamide] memristor, *J. Mater. Chem. C* **11**, 17093 (2023).
- [22] Y. R. Panthi, A. Pandey, A. Šturcová, D. Výprachtický, S. H. Foulger, and J. Pflieger, Emulating synaptic plasticity with poly(n-(3-(9h-carbazol-9-yl)propyl)methacrylamide) memristor, *Mater. Adv.* (2024).
- [23] B. Grant, Y. Bandera, S. H. Foulger, J. Vilčáková, P. Sába, and J. Pflieger, Boolean and elementary algebra with a roll-to-roll printed electrochemical memristor, *Adv. Mater. Technol.* **7**, 2101108 (2022).

- [24] S. H. Foulger, Y. Bandera, T. Wanless, I. Luzinov, O. Cobb, M. G. Sehorn, L. Kostal, J. Pflieger, and J. Vilčáková, Towards a hardware spiking neural network: Learning and adaptation with an environmentally sustainable polymer memristor (2025), submitted.
- [25] S. Ostošic and N. Brunel, From Spiking Neuron Models to Linear-Nonlinear Models, *PLoS Comput. Biol.* **7**, e1001056 (2011).
- [26] A sufficient condition is that k , H are of bounded variation and vanish for negative times, which is the case for the functions we are considering.
- [27] We require of H that it be differentiable almost everywhere.
- [28] S. Tang, F. Tesler, F. Gomez Marlasca, P. Levy, V. Dobrosavljević, and M. Rozenberg, Shock waves and commutation speed of memristors, *Phys. Rev. X* **6**, 011028 (2016).
- [29] W. Gerstner, M. Lehmann, V. Liakoni, D. Corneil, and J. Brea, Eligibility traces and plasticity on behavioral time scales: Experimental support of neohebbian three-factor learning rules, *Front. Neural Circuits* **12**, 53 (2018).
- [30] S. Kirkpatrick, Percolation and conduction, *Rev. Mod. Phys.* **45**, 574 (1973).
- [31] H. Scher and M. Lax, Stochastic transport in a disordered solid. i. theory, *Phys. Rev. B* **7**, 4491 (1973).
- [32] S. H. Foulger, Y. Bandera, I. Luzinov, and T. Wanless, Polymeric memristors as entropy sources for probabilistic bit generation, *Adv. Phys. Res.* **4**, 2400142 (2025).